Gyrokinetic turbulence simulations with kinetic electrons*

Yang Chen[†,a)] and Scott Parker
Center for Integrated Plasma Studies, Department of Physics, University of Colorado at Boulder, Boulder, Colorado 80309

(Received 23 October 2000; accepted 3 January 2001)

Gyrokinetic turbulence simulations are presented with full drift-kinetic electron dynamics including both trapped and passing particle effects. This is made possible by using a generalization of the split-weight scheme [I. Manuilskiy and W. W. Lee, Phys. Plasmas **7**, 1381 (2000)] that allows for a variable adiabatic part, as well as use of the parallel canonical momentum formulation. Linear simulations in shearless slab geometry and nonlinear simulations using representative tokamak parameters demonstrate the applicability of this generalized split-weight scheme to the turbulence transport problem in the low β regime $[\beta(m_i/m_e)\leqslant 1]$. The issues relating to difficulties at higher β, and initial three-dimensional toroidal simulations results will be discussed. © *2001 American Institute of Physics.* [DOI: 10.1063/1.1351828]

I. INTRODUCTION

Accurately modeling the electron physics is currently a primary challenge in turbulence simulation research. Up until recently, the vast majority of three-dimensional simulations in realistic geometries have been using the adiabatic electron approximation. Recently, a split-weight scheme has been proposed for the treatment of kinetic electrons in gyrokinetic simulations.[1] The scheme, which is based on the δf method, splits the kinetic electron response into adiabatic and nonadiabatic parts. The separation of the adiabatic part introduces another moment equation, derived from the gyrokinetic Poisson equation, into the scheme. However, this separation allows us to circumvent the restriction of the Courant condition[2] on the time step. The validity of the scheme has been demonstrated in a one-dimensional (1-D) electrostatic simulation for the drift waves. It is of immediate interest to study the efficacy of this scheme in the more complicated problem of three-dimensional (3-D) toroidal simulations with electromagnetic perturbations, which is the purpose of the present article.

The magnetic perturbation considered in this article is given by a parallel vector potential $A_\parallel$, $\delta\mathbf{B}_\perp=\nabla A_\parallel\times\mathbf{b}$, where $\mathbf{b}$ is the unit vector along the equilibrium magnetic field. It is known that the inductive component of the electric field perturbation, $\partial A_\parallel/\partial t$, introduces a numerical difficulty in particle simulation, which has lead to two approaches in previous simulations.[3] The first approach employs a generalized Ohm's law to calculate the parallel electric field.[4] More recent simulations usually use the second approach which uses the parallel canonical momentum formulation to eliminate $\partial A_\parallel/\partial t$ from the equations.[5–7] Both approaches can be adopted in the split-weight scheme and are considered in this article. Here, we formulate a generalized split-weight scheme where the adiabatic part (either $p_\parallel$ or $v_\parallel$), as well as comparisons with exact linear theory to determine the best performing approach. Finally, we show initial nonlinear toroidal results which demonstrate the new kinetic electron physics capability.

The article is organized as follows: In Sec. II we present a generalized electromagnetic split-weight scheme using both the $p_\parallel$ and the $v_\parallel$ formulations. Methods for implementation are given in Sec. III. In Sec. IV the numerical scheme is tested for both the shearless slab, where detailed comparison with dispersion relation is possible, and the toroidal flux-tube geometry, showing that at low β, the nonadiabatic electron effect of interest can be adequately addressed using the split-weight scheme. Main conclusions of the article are given in Sec. V.

II. THE SPLIT-WEIGHT SCHEME

We start with the collisionless gyrokinetic equation,

$$\frac{\partial f_\alpha}{\partial t}+\mathbf{v}_{G\alpha}\cdot\nabla f_\alpha+\dot{v}_{\parallel\alpha}\frac{\partial f_\alpha}{\partial v_\parallel}=0, \tag{1}$$

where $\alpha=i,e$. Here $\dot{v}_{\parallel\alpha}=(q_\alpha/m_\alpha)(-\tilde{\mathbf{b}}\cdot\nabla\langle\phi\rangle-\partial\langle A_\parallel\rangle/\partial t)-(\mu_\alpha/m_\alpha)\tilde{\mathbf{b}}\cdot\nabla B+v_{\parallel\alpha}(\mathbf{b}\cdot\nabla\mathbf{b})\cdot\mathbf{v}_E$, $\mathbf{v}_{G\alpha}=v_{\parallel\alpha}\tilde{\mathbf{b}}+\mathbf{v}_{d\alpha}+\mathbf{v}_E$ is the guiding center velocity. $\tilde{\mathbf{b}}=\mathbf{b}+\langle\delta\mathbf{B}_\perp\rangle/B$, $\mathbf{v}_{d\alpha}=[(v_\parallel^2+v_\parallel^2/2)/\Omega_\alpha B^2]\mathbf{B}\times\nabla B$ is the drift velocity for low-β tokamak plasmas with $\beta\ll 1$, $\mathbf{v}_E=\langle\mathbf{E}\rangle\times\mathbf{b}/B$. In this article the electrons are described by the drift-kinetic equations due to their small gyro radii, hence $\langle\phi\rangle=\phi$, etc., for electrons.

In the canonical momentum formulation,[8] the parallel canonical momentum $p_{\parallel\alpha}=v_{\parallel\alpha}+(q_\alpha/m_\alpha)\langle A_\parallel\rangle$ is used instead of $v_\parallel$,

$$\dot{p}_{\parallel\alpha}=-\frac{q_\alpha}{m_\alpha}\tilde{\mathbf{b}}\cdot\nabla\langle\phi\rangle-\frac{\mu_\alpha}{m_\alpha}\tilde{\mathbf{b}}\cdot\nabla B+v_{\parallel\alpha}(\mathbf{b}\cdot\nabla\mathbf{b})\cdot\mathbf{v}_E+\frac{q_\alpha}{m_\alpha}\mathbf{v}_{G\alpha}\cdot\nabla\langle A_\parallel\rangle. \tag{2}$$

*Paper HI2 4, Bull. Am. Phys. Soc. **45**, 159 (2000).
†Invited speaker.
a)Electronic mail: yang.chen@colorado.edu

The ions are simulated using the usual δf method. Define $f_i = f_{0\mathrm{i}} + \delta f_i$ with $f_{0\alpha}$ the Maxwellian distribution in $p_{\parallel\alpha}$ ($\varepsilon_\alpha = m_\alpha(v_{\perp\alpha}^2 + p_{\parallel\alpha}^2)/2$),

$$f_{0\alpha} = \frac{n_{0\alpha}}{(2\pi)^{3/2} v_{\mathrm{t}\alpha}^3} e^{-\varepsilon_\alpha/T_\alpha}. \tag{3}$$

Here δf_i evolves according to

$$\frac{d\,\delta f_i}{dt} = -\left(v_{\parallel i}\frac{\delta \mathbf{B}_\perp}{B} + \mathbf{v}_E\right)\cdot \nabla f_{0\mathrm{i}} - \dot{\varepsilon}_i \frac{\partial f_{0\mathrm{i}}}{\partial \varepsilon_i}, \tag{4}$$

where $\dot{\varepsilon}_i = \mu_i \mathbf{v}_{\mathrm{Gi}}\cdot\nabla B + m_i p_{\parallel i}\dot{p}_{\parallel i}$.

A fraction of the adiabatic part of the electrons perturbed distribution is treated separately in the split-weight scheme. Thus we write

$$f_e = f_{0\mathrm{e}} - \epsilon_g e\phi\frac{\partial f_{0\mathrm{e}}}{\partial \varepsilon_e} + h. \tag{5}$$

Here we have generalized the split-weight scheme so that the part of the distribution separated can be adjusted by a parameter ϵ_g. The original split-weight scheme[1] corresponds to the case with $\epsilon_g = 1$. If it turns out that the enhancement of time step relies crucially on the explicit treatment of all the adiabatic response ($\epsilon_g = 1$), this free parameter will be of little use. We will address this issue in Sec. III when we perform numerical tests of the split-weight scheme. We also note that the adiabatic contribution associated with $A_\parallel$ is not separated from the electron distribution here, as has been proposed by Lee. That separation will necessitate the calculation of $\partial A_\parallel/\partial t$, and hence contradicts the purpose of the $p_\parallel$ formulation.

The distribution h evolves according to

$$\begin{aligned}\frac{dh}{dt} = &-\left(v_{\parallel e}\frac{\delta \mathbf{B}_\perp}{B} + \mathbf{v}_E\right)\cdot\nabla f_{0\mathrm{e}} - \dot{\varepsilon}_e\frac{\partial f_{0\mathrm{e}}}{\partial \varepsilon_e}\\ &+ \epsilon_g e\left[\left(\frac{\partial \phi}{\partial t} + \mathbf{v}_{\mathrm{Ge}}\cdot\nabla\phi\right)\frac{\partial f_{0\mathrm{e}}}{\partial \varepsilon_e}\right.\\ &\left.+ \phi\left(\mathbf{v}_{\mathrm{Ge}}\cdot\nabla + \dot{\varepsilon}_e\frac{\partial}{\partial \varepsilon_e}\right)\frac{\partial f_{0\mathrm{e}}}{\partial \varepsilon_e}\right].\end{aligned} \tag{6}$$

As can be seen from Eq. (6), one need calculate the quantity $\partial\phi/\partial t$ in the split-weight scheme. It is possible to calculate this quantity using a finite difference method.[9] Following Manuilsky and Lee,[1] we will derive a moment equation for $\dot{\phi} = \partial\phi/\partial t$ from the quasi-neutrality form of the gyrokinetic Poisson equation,[10]

$$\begin{aligned}&n_{0\mathrm{i}}\frac{q_i^2}{T_i}(\phi - \tilde{\phi}) + \epsilon_g n_{0\mathrm{e}}\frac{e^2}{T_e}\phi\\ &= q_i\int \delta f_i \delta(\mathbf{R}+\rho-\mathbf{x})\,d\mathbf{R}\,d\mathbf{v} - e\int h\,d\mathbf{v}.\end{aligned} \tag{7}$$

Taking the time derivative of Eq. (7), using the continuity form of the original gyrokinetic equation (1), we obtain

$$\begin{aligned}&n_{0\mathrm{i}}\frac{q_i^2}{T_i}(\dot{\phi} - \dot{\tilde{\phi}})\\ &= -\nabla\cdot q_i\int f_i \mathbf{v}_{\mathrm{Gi}}\delta(\mathbf{R}+\rho-\mathbf{x})\,d\mathbf{R}\,d\mathbf{v} + \nabla\cdot e\int f_e\mathbf{v}_{\mathrm{Ge}}\,d\mathbf{v}.\end{aligned} \tag{8}$$

In Eq. (7) $\tilde{\phi}$ is defined as

$$\tilde{\phi} = \sum_{\mathbf{k}} \Gamma_0(k_\perp^2 v_{\mathrm{ti}}^2/\Omega_i^2)\,\phi_k \exp(i\mathbf{k}\cdot\mathbf{x}) \tag{9}$$

with $\phi = \Sigma_{\mathbf{k}}\phi_k\exp(i\mathbf{k}\cdot\mathbf{x})$. $\dot{\phi}$ and $\dot{\tilde{\phi}}$ are similarly defined. Equation (8) can be expressed in terms of δf_i and h as

$$\begin{aligned}n_{0\mathrm{i}}\frac{q_i^2}{T_i}(\dot{\phi} - \dot{\tilde{\phi}}) = &\, n_{0\mathrm{e}}\frac{e^2}{m_e}\nabla_\parallel A_\parallel - \epsilon_g\nabla\cdot\int e^2\phi\frac{\partial f_{0\mathrm{e}}}{\partial \varepsilon_e}\mathbf{v}_{\mathrm{Ge}}\,d\mathbf{v}\\ &- \nabla\cdot q_i\int \delta f_i\mathbf{v}_{\mathrm{Gi}}\delta(\mathbf{R}+\rho-\mathbf{x})\,d\mathbf{R}\,d\mathbf{v}\\ &+ \nabla\cdot e\int h\mathbf{v}_{\mathrm{Ge}}\,d\mathbf{v} - \nabla\cdot\left(q_i\int f_{0\mathrm{i}}\frac{\langle\mathbf{E}\rangle\times\mathbf{b}}{B}\right.\\ &\left.\times\delta(\mathbf{R}+\rho-\mathbf{x})\,d\mathbf{R}\,d\mathbf{v} - e\int f_{0\mathrm{e}}\frac{\mathbf{E}\times\mathbf{b}}{B}d\mathbf{v}\right).\end{aligned} \tag{10}$$

The last two terms on the right-hand-side (RHS) of Eq. (10) do not cancel each other due to the ion Larmor radius effect. Ion contributions that are a factor of m_e/m_i smaller than corresponding electron terms are neglected in Eq. (10).

Neglecting the contribution of $-\epsilon_g e\phi(\partial f_{\mathrm{oe}}/\partial\varepsilon_e)$ to parallel current, which is proportional to $\phi A_\parallel$, Ampere's law is

$$\begin{aligned}&\left(-\nabla_\perp^2 + \frac{\omega_{\mathrm{pe}}^2}{c^2}\right)A_\parallel\\ &= \mu_0\left(q_i\int \delta f_i v_\parallel\delta(\mathbf{R}+\rho-\mathbf{x})\,d\mathbf{R}\,d\mathbf{v} - e\int h v_\parallel\,d\mathbf{v}\right).\end{aligned} \tag{11}$$

We note that in $p_\parallel$-formulation $v_\parallel$ need be computed from $p_\parallel$ and $A_\parallel$, hence Eq. (11) contains terms of the form $\delta n_\alpha A_\parallel$, which is nonlinear and requires an iterative procedure for solving Eq. (11).[5] In this article such nonlinear terms are neglected. Equations (4), (6), (7), (10), and (11) complete the $p_\parallel$ formulation of the split-weight scheme.

For the comparison of simulations with dispersion relation in Sec. IV, we also provide the equations for the $v_\parallel$ formulation in a shearless slab. When $v_\parallel$ is used as the coordinate, $f_{0\alpha}$ is defined as Maxwellian in terms of $v_\parallel$ and the electron distribution function is still split as Eq. (5). Evolution equations for δf_i and h are trivially obtained. Linearly the equation for $\dot{\phi}$ is identical to Eq. (10) except that the $A_\parallel$ term on the right-hand side of Eq. (10) should be removed, since f_0 does not carry a current. The $\omega_{\mathrm{ps}}^2/c^2 A_\parallel$ term is removed from Ampere's law due to the same reason. The main difference between the two formulations is the appearance of an equation for $\dot{A}_\parallel$. This equation is derived from taking the

time derivative of Ampere's law and using the kinetic (1) to eliminate $\partial f_\alpha/\partial t$. The result is, for a shearless slab,

$$\left(-\nabla_\perp^2+\frac{\omega_{\rm pe}^2}{c^2}\right)\dot{A}_\parallel = -\mu_0\nabla_\parallel\left(q_i\int v_\parallel^2\delta f_i\delta(\mathbf{R}+\rho-\mathbf{x})\,d\mathbf{R}\,d\mathbf{v}-e\int v_\parallel^2 h\,d\mathbf{v}\right) + \mu_0\frac{e}{m_e}[\delta\mathbf{B}_\perp\cdot(n_{0e}T_{0e})-(1-\epsilon_g)\nabla_\parallel\phi]. \quad (12)$$

Nonlinear terms have been neglected. Although f_{0e} does not contribute to electric current, it contributes the term $\omega_{\rm pe}^2/c^2\dot{A}_\parallel$ in the above equation. Again ion terms that are a factor of m_e/m_i smaller than the corresponding electron terms are neglected.

III. IMPLEMENTATION

The $p_\parallel$-formulation of the split-weight scheme has been implemented in a toroidal field-line-following flux-tube geometry.[11] The coordinates are defined by $x=r-r_0$, $y=(r_0/q_0)q\,\theta-\zeta)$ and $z=q_0R_0\theta$, with (r,θ,ζ) the usual toroidal coordinates. r_0 is the radius of the center of the flux-tube, $q(r)$ is the safety factor, and $q_0=q(r_0)$. Unshifted circular flux surfaces are assumed. In the following we use ρ_i as the unit of length, $\rho_i/v_{\rm Ti}$ as the unit of time, $T_i/e\rho_i$ as the unit of electric field, and B_0 as the unit of magnetic field. The simulation domain $(0,l_x)\times(0,l_y)\times(0,l_z)$ is chosen such that $l_z=2\pi q_0R_0$. Periodical boundary conditions are used in x and y directions, while the toroidal boundary condition[11] is used in z.

A predictor–corrector scheme is used for evolving the particle trajectories and field equations. After each predictor or corrector step of particle pushing, the Poisson equation and Ampere's law, Eqs. (7) and (11), are solved sequentially using spectral methods. Once ϕ and $A_\parallel$ are available, Eq. (10) can be solved similar to the Poisson equation. Using the field-line-following coordinates, the second term on the RHS of Eq. (10) is, in dimensionless units,

$$-\epsilon_g\nabla\int\phi\frac{\partial f_{0e}}{\partial\varepsilon_e}\mathbf{v}_{Ge}\,d\mathbf{v} = \epsilon_g\frac{2}{R_0}\left(\frac{\partial\phi}{\partial x}\sin\theta+\frac{\partial\phi}{\partial y}(\cos\theta+s_z\sin\theta)\right). \quad (13)$$

Terms nonlinear in ϕ have been neglected. The last term on the RHS of Eq. (10) can be expressed as, for $q=e=1$,

$$\nabla\cdot\left(\int f_{0i}\frac{\langle\mathbf{E}\rangle\times\mathbf{b}}{B}\delta(\mathbf{R}+\rho-\mathbf{x})\,d\mathbf{R}\,d\mathbf{v}-\int f_{0e}\frac{\mathbf{E}\times\mathbf{b}}{B}d\mathbf{v}\right) = \frac{n_0\kappa_n}{B_0}\sum_{k_x,k_y} ik_y(\Gamma_0(b)-1)\phi_{k_x,k_y}\exp i(k_xx+k_yy) \quad (14)$$

with $n_{0i}=n_{0e}=n_0$, $\kappa_n=-(\partial n_0/\partial x)/n_0$, $b=(k_x^2+k_y^2(1+s_z^2)+2k_xk_ys_z)/B(z)^2$, $s_z=(r_0/q_0)q'\theta$. This quantity can be conveniently evaluated inside the Poisson solver where ϕ_{k_x,k_y} is available.

For numerical comparison the $v_\parallel$ formulation is also implemented in a shearless slab geometry. In this case the equation for $\partial A_\parallel/\partial t$, Eq. (12), is solved in a way similar to Ampere's law.

IV. NUMERICAL STUDY OF THE SPLIT-WEIGHT SCHEME

A. Shearless slab simulations

Consider a slab of plasma with constant equilibrium magnetic field $\mathbf{B}=B_0\hat{\mathbf{z}}$. Plasma density $n_0(x)$ and temperature $T_{i0}(x)$, $T_{e0}(x)$ are nonuniform in the x direction. Here we assume $T_{0i}=T_{0e}$ but allow different temperature gradients for electrons and ions. For the purpose of comparing simulations with analytical results in detail, we provide below the fully kinetic electromagnetic dispersion relation for such a shearless slab,[4]

$$-k_\perp^2\frac{k_\parallel}{\omega}(M_i-M_e-k'^2_\perp)=\beta(N_e-N_i)(k'^2_\perp-L_i+L_e), \quad (15)$$

where $\beta=v_{\rm ti}^2/v_{\rm A}^2$ and $v_{\rm A}^2=B_0^2/\mu_0n_0m_i$ is the Alfvén velocity. Other quantities in Eq. (15) are defined as the following: $L_i=(\Omega-\Omega_{\rm Ti})\Gamma_0+\Omega_{\rm Ti}\Gamma_*$, $M_i=-\Gamma_0(1+\zeta_iZ_i)+(\frac{3}{2}\Omega_{\rm Ti}\Gamma_0-\Omega_{\rm Ti}\Gamma_*-\Omega\Gamma_0)\zeta_iZ_i-\Omega_{\rm Ti}\Gamma_0\zeta_i^2(1+\zeta_iZ_i)$, $N_i=-(\omega/k_\parallel)\times[\Omega\Gamma_0(1+\zeta_iZ_i)+(-\frac{3}{2}\Omega_{\rm Ti}\Gamma_0+\Gamma_0+\Omega_{\rm Ti}\Gamma_*)(1+\zeta_iZ_i)+\Omega_{\rm Ti}\Gamma_0(\frac{1}{2}+\zeta_i^2+\zeta_i^3Z_i)]$, $L_e=\Omega$, $M_e=1-(\Omega-\Omega_{\rm Te}/2-1)\zeta_eZ_e(\zeta_e)-\Omega_{\rm Te}\zeta_e^2(1+\zeta_eZ_e)$, $N_e=-(\omega/k_\parallel)[\Omega_{\rm Te}(\frac{1}{2}+\zeta_e^2(1+\zeta_eZ_e))+(\Omega-\Omega_{\rm Te}/2-1)(1+\zeta_eZ_e)]$, $\kappa_n=-(dn_0/dx)/n_0$, $\kappa_{T\alpha}=-(dT_{0\alpha}/dx)/T_0$, $\Omega=\kappa_nk_y/\omega$, $\Omega_{T\alpha}=\kappa_{T\alpha}k_y/\omega$, $\Gamma_0=\Gamma_0(b)=\Gamma_0(k_\perp^2v_{\rm ti}^2/\Omega_i^2)$, $\Gamma_*=\Gamma_0-b(\Gamma_0-\Gamma_1)$, and $k'^2_\perp=1-\Gamma_o(b)$. $\zeta_\alpha=\omega/\sqrt{2}k_\parallel v_{t\alpha}$ and $Z_\alpha=Z(\zeta_\alpha)$ is the plasma dispersion function.

Equation (15) is solved numerically for $\omega(\mathbf{k})$ and the results are compared with simulations for ion-temperature-gradient-driven (ITG) modes, electron drift waves, and Alfvén waves. The box size for the shearless slab simulations is $l_x=l_y=64$, $l_z=3140$; typically 524 288 particles are used. The grid resolution is $64\times64\times32$. For better comparison with the dispersion relation only a single Fourier mode (including its complex conjugates) is retained. All the simulations are performed with $q=e$, $T_{0i}=T_{0e}$, and $m_i/m_e=1837$.

Figure 1 shows the measure mode frequencies versus κ_n for $\beta=10^{-4}$, $\kappa_{\rm Ti}=0.1$, and $\kappa_{\rm Te}=0.01$. The mode wave number is $k_x=0.1$, $k_y=0.3$, and $k_\parallel=0.002$. Time step is $\Delta t=4$. The mode growth rates are plotted in Fig. 2. Simulation results with both $\epsilon_g=1$ (stars) and $\epsilon_g=0.1$ (diamonds) are shown, together with the solution of the dispersion relation. As κ_n increases, the dominant mode shifts from the ITG mode to the drift wave. Near $\kappa_n=0.05$ both modes are unstable and the simulation nicely picks up the mode with larger growth rate, as can be clearly seen from the observed mode frequency. Good agreement between theory and simulation is seen for the wave frequency and growth rate, except in the case of $\epsilon_g=1$ the growth rate of the drift wave significantly deviates from that predicted by the dispersion relation. Thus the choice $\epsilon_g=1$, which corresponds to the

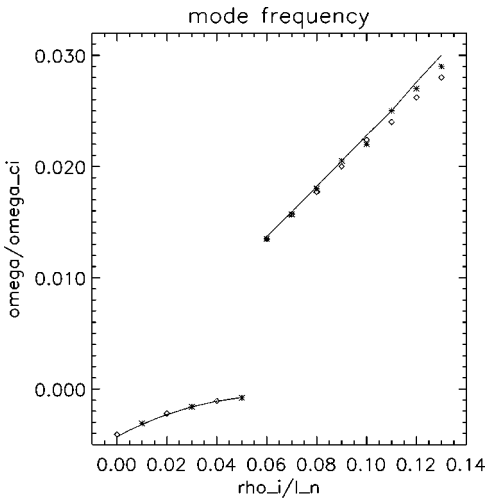

FIG. 1. Linear simulation results of mode frequency for both drift waves (upper) and ITG modes (lower) agree well with solutions of the dispersion relation (solid line). Diamonds are results of simulations using $p_\parallel$ formulation, stars are results of simulations using $v_\parallel$ formulation.

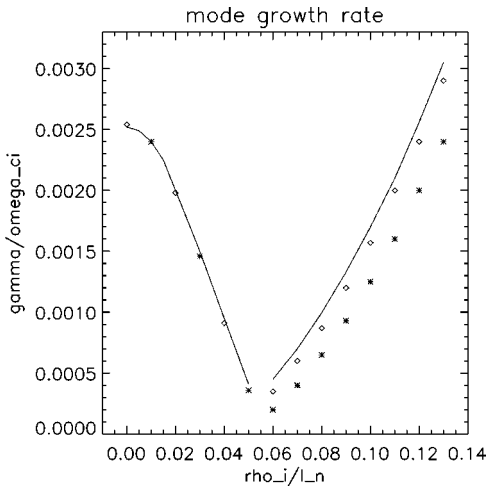

FIG. 2. Mode growth rates versus density gradient. The left curve is for ITG modes, right for drift waves. For the drift wave branch, results of simulations using $\epsilon_g=0.1$ agree better with the dispersion relation than that using $\epsilon_g=1$.

original split-weight scheme proposed by Manuilskiy and Lee,[1] is not always optimal if accuracy is desired. However, in the case of ITG modes, the choice $\epsilon_g=1$ is appropriate. The restriction on the time step depends on the choice of ϵ_g. Numerical experiments show that, for the case with $\kappa_n=0.01$, numerical stability requires that $\Delta t\leqslant 10$ ($k_\parallel v_{\mathrm{Te}}\Delta t\leqslant 0.9$) for $\epsilon_g=1$, $\Delta t\leqslant 6$ for $\epsilon_g=0.1$, and $\Delta t\leqslant 2.5$ for $\epsilon_g=0$.

As will be seen later in the discussion of toroidal simulations, the increase in time step due to the split-weight scheme is more dramatic in nonlinear simulations where a large number of Fourier modes are retained. Here we summarize the following observations regarding the effect of the split-weight scheme on the time step: (a) the fact that a small ϵ_g allows a large increment in Δt indicates that, as far as the time step is concerned, it is not crucial for the explicit term in Eq. (5) to catch the full adiabatic response (e.g., $\epsilon_g=1$ for $\beta=0$). (b) The allowed maximal time step without causing numerical instabilities increases with β. In some cases, the condition $\omega_{\mathrm{A}}\Delta t\leqslant 1$ for numerical stability[2,1] (ω_{A} is the Alfvén wave frequency) can be violated without causing numerical instability. (c) The Courant condition $k_\parallel v_{\mathrm{Te}}\Delta t\leqslant 1$ can indeed be violated while the mode frequency and growth rate of interest are still accurately calculated. The observations (b) and (c) can be demonstrated for the ITG mode in Figs. 1 and 2 with $\beta=4\times10^{-4}$, $\epsilon_g=1$, and $\kappa_n=0.01$. The frequency and growth rate of the ITG mode are little changed by the small β. Simulation with a time step of $k_\parallel v_{\mathrm{Te}}\Delta t=1.37$ ($\omega_{\mathrm{A}}\Delta t\approx 1.6$) gives $\omega=(-3.3\times10^{-3},2.3\times10^{-3})$, in good agreement with the dispersion relation. However, as is expected when $\omega_{\mathrm{A}}\Delta t>1$, the Alfvén wave is not correctly simulated with such a large time step. Thus in the presence of both the Alfvén wave and the drift instabilities, the split-weight scheme allows us to sacrifice the accuracy of the Alfvén wave for the efficient simulation of the drift waves, if this is desired.

The deviation between the dispersion relation and simulation results at large ϵ_g is indicative of a more general problem. In conventional δf simulations all the electron density response is computed from δf. This density response, when computed from δf, is subject to the effect of finite particle size and finite grid size,[2] regardless of whether an electron is adiabatic or nonadiabatic. However, in the split-weight scheme, the contribution of the part of distribution $-\epsilon_g e\phi\partial f_{\mathrm{oe}}/\partial\varepsilon$ to the electron density, $\epsilon_g n_0 e\phi/T_0$, is known analytically in the Poisson equation, Eq. (7), without being subject to the effect of finite particle and grid size, as is the case for h, the rest of the distribution. We believe that it is such unequal treatments of different parts of the distribution that causes the deviation between theory and simulations at large ϵ_g. In this regard the terms proportional to $\omega_{\mathrm{pe}}^2/c^2$ in Eq. (11) for the $p_\parallel$-formulation and in Eq. (12) for the $v_\parallel$ formulation are similar to the ϵ_g term in the Poisson equation, and hence can be expected to cause inaccuracy at large $\beta m_i/m_e=\omega_{\mathrm{pe}}^2/c^2$.

Figure 3 shows the simulation results for the Alfvén wave frequency at different β. In this case $\kappa_n=\kappa_{\mathrm{Ti}}=\kappa_{\mathrm{Te}}=0$, $\epsilon_g=1$, and $\Delta t=1$. Results from both the $p_\parallel$-formulation (diamonds) and the $v_\parallel$-formulation (stars) are shown. The frequency at $\beta=0$ is the electrostatic Alfvén wave[12] given by $\omega_H^2=(k_\parallel^2/k_\perp^2)v_{\mathrm{te}}^2$. The results with $p_\parallel$-formulation agree well with the dispersion relation for $\beta m_i/m_e\leqslant 2$. However, at large β significant deviation is seen. The results from $v_\parallel$-formulation deviate from the dispersion relation even more. This observation at large β was previously seen in one-dimensional gyrokinetic particle simulations.[5] It was also observed in Vlasov simulations[13] using the $p_\parallel$-formulation, where the finite grid effects are also present, although no particles are used. It had been suggested that one needs to resolve the magnetic skin depth, $\delta_s=\sqrt{m_e/\beta m_i}$, to correctly reproduce any finite β effect at large β.

Finite β effects are shown in Fig. 4 where the frequencies and growth rates of the drift wave are plotted versus β. In this case $l_x=l_y=64$, $l_z=6280$, and mode wave number is $k_x=0.2$, $k_y=0.4$ and $k_\parallel=0.001$. Other parameters are κ_{Ti}

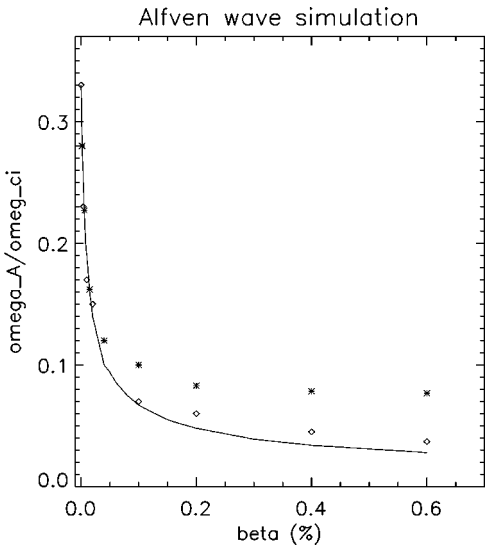

FIG. 3. Alfvén wave frequency vs β. At large β, simulation results differ from the dispersion relation.

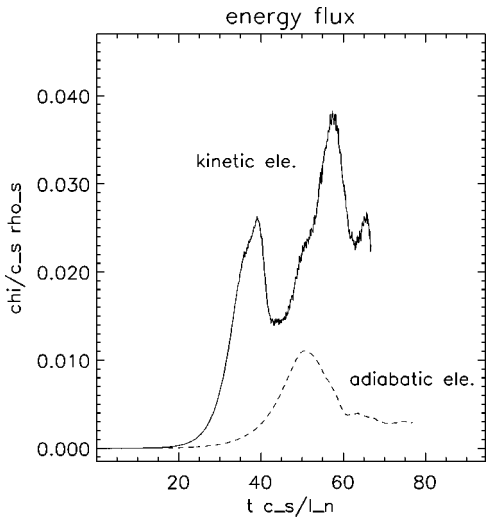

FIG. 5. Evolution of ion heat diffusivity for the DIII-D Base Case parameters. The maximum growth rate increases from the adiabatic simulation by 70%, the saturated ion flux is increases by more than five times.

$=\kappa_{\mathrm{Te}}=0$, $\kappa_n=0.1$, $\epsilon_g=0.2$, and $\Delta t=4$. Finite β stabilization can be observed, but the difference between simulation results and the dispersion relation is apparent.

B. Toroidal simulations

It is clear from the above discussion that finite β effects in a typical tokamak plasma with $\beta m_i/m_e \geqslant 1$ cannot be adequately simulated using the electromagnetic simulation scheme presented here, regardless of whether the split-weight scheme is used. However, within the low-β regime $\beta m_i/m_e \leqslant 1$ the split-weight scheme *does* afford us the capability of simulating the full electron dynamics in a toroidal geometry, including nonadiabatic effects of the passing electrons and the trapped electron effects. The advantage of the split-weight scheme over the conventional δf method is more clearly seen in the nonlinear simulations where a large number of Fourier modes are present. We have seen previously that for a particular case the time step is enhanced from $k_\parallel v_{\mathrm{te}} \Delta t \leqslant 0.25$ without the split-weight scheme to $k_\parallel v_{\mathrm{te}} \Delta t \leqslant 1$ with the split-weight scheme. This result of single mode simulation is somewhat misleading. In our nonlinear simulations, both in shearless slab geometry and in toroidal geometry, we have observed nonlinear saturation with a typical time step of $\Delta t \Omega_i > 1$ using the split-weight scheme, whereas without the split-weight scheme the simulation is numerically unstable even with a time step ~ 10 times smaller. In these nonlinear simulations all the modes with $k_\perp \leqslant 1$ are retained, while in the parallel direction the digital filtering is applied to the particle density and parallel current.

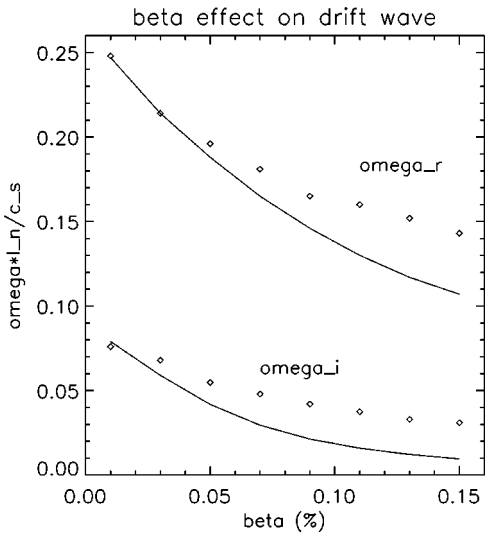

FIG. 4. Mode frequency (upper) and growth rate (lower) vs β for the drift wave. Finite β stabilization is difficult to see in simulations when $\beta m_i/m_e \geqslant 1$.

We first study the ITG instability in a torus with the ''DIII-D[14] Base Case'' parameters: $R_0\kappa_{\mathrm{Ti}}=6.9$, $R_0\kappa_n=2.2$, $T_i=T_e$, $r_0/R_0=0.18$, $q_0=1.4$, and $\hat{s}=(r_0/q_0)(dq/dr)=0.78$. We choose $\kappa_{\mathrm{Te}}=0$. The size of the flux tube is $l_x \times l_y \times l_z = 64\rho_i \times 64\rho_i \times 2\pi q_0 R_0$, and grid resolution is $64 \times 64 \times 32$. Particle number is 1 048 576. Although the realistic plasma β is not accessible, we find, surprisingly, that a small β ($\beta=10^{-4}$) allows us to use a relatively large time step, $\Delta t \Omega_i \leqslant 5$ for $\epsilon_g=0.3$, compared with the requirement $\Delta t \Omega_i \leqslant 1$ for $\beta=0$. This might be due to the large ω_H mode frequency at $\beta=0$. $\epsilon_g<1$ is chosen since we are interested in cases where accurate electron dynamics is desired. Figure 5 shows the evolution of the ion energy flux. Results from both kinetic electron simulation and simulation with adiabatic electrons are shown. The linear growth rate estimated from the field energy is $\gamma L_n/c_s \approx 0.15$, about 70% increased from the adiabatic electron result. The steady-state ion energy flux cannot be determined as accurately in the kinetic electron simulation as in the adiabatic run. If the ion heat diffusivity is taken to be $0.022 c_s \rho_i$, it is increased from that of the adiabatic run by more than a factor of 5. This result indicates that the effect of nonadiabatic electrons on the ion transport is not negligible. On the other hand, the particle flux, which is ambipolar intrinsically due to the quasi-neutrality condi-

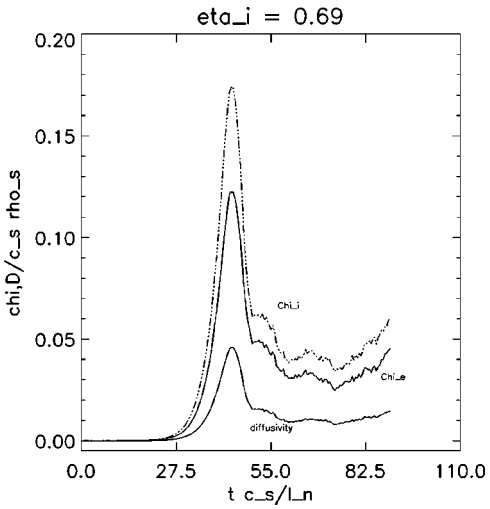

FIG. 6. As the density gradient is increased from the Base Case so that $\eta_i = 0.69$, trapped electron driven instability is observed. Significant particle flux and electron heat flux are observed in the saturated states.

tion, is negligible compared with the ion energy flux for this set of parameters, as would be implied by adiabatic electrons. The electron energy flux is also negligible in this case.

As we increase density gradient from the Base Case value to $\kappa_n \rho_i = 0.01$ ($\eta_i = 0.69$) the instability shifts from predominantly ion driven to electron driven, and we can observe significant particle flux and electron energy flux. Figure 6 shows the evolution of the particle flux and the energy flux of both species. Other parameters are the same as in Fig. 5 except $\kappa_{\mathrm{Te}} \rho_i = 0.005$. The simulation with adiabatic electrons show that the plasma is stable as expected. The instability observed is clearly driven by nonadiabatic electrons, as can be seen from examining the trapped particle contribution of the particle flux, which dominates the passing electrons.

V. CONCLUSION

We have developed an electromagnetic, gyrokinetic ion, and drift-kinetic electro-particle simulation model in three-dimensional toroidal field-line-following geometry, using a generalized split-weight scheme[1] and the parallel canonical momentum formulation.[8,5] The original split-weight scheme[1] has been modified so that the adiabatic part of the particle distribution can be varied. This helps improve accuracy in drift wave simulations. We have performed detailed comparisons between shearless slab simulations and the linear dispersion relation for kinetic Alfvén waves, ITG modes, and drift waves. It is shown that the split-weight scheme can greatly increase the time step in simulations. Most importantly, it now makes it possible for nonlinear toroidal simulation of tokamak plasma microturbulence with full electron dynamics keeping the full $k_\parallel$ and $k_\perp$ wave spectrum. We have also begun to quantify inaccuracy problems at large β, which have been previously observed in electromagnetic simulations with finite spatial resolution,[5,13] and have shown errors that persist regardless of which formulation ($v_\parallel$ or $p_\parallel$) is used. More work is needed to address the moderate β plasmas where both fully kinetic electrons and electromagnetic effects are important.

ACKNOWLEDGMENTS

We would like to thank Dr. Bruce Cohen for helpful discussions.

This work is supported by the U.S. Department of Energy, Office of Fusion Energy Sciences.

[1] I. Manuilsky and W. W. Lee, Phys. Plasmas **7**, 1381 (2000).
[2] C. Birdsall and A. Longdon, *Plasma Physics Via Computer Simulation* (McGraw-Hill, New York, 1985).
[3] C. Nielson and H. Lewis, Methods Comput. Phys. **16**, 367 (1976).
[4] J. Reynders, Ph.D. thesis, Princeton University, 1992.
[5] J. Cummings, Ph.D. thesis, Plasma Physics Lab, Princeton University, 1994.
[6] B. Cohen and A. Dimits, Phys. Rev. E **56**, 2151 (1997).
[7] H. Naitou, K. Tsuda, W. Lee, and R. Sydora, Phys. Plasmas **2**, 4257 (1995).
[8] T. S. Hahm, W. W. Lee, and A. Brizard, Phys. Fluids **31**, 1940 (1988).
[9] B. Cohen, private communication (2000).
[10] W. W. Lee, Phys. Fluids **26**, 556 (1983).
[11] M. A. Beer, S. C. Cowley, and G. W. Hammett, Phys. Plasmas **2**, 2687 (1995).
[12] W. W. Lee, J. Comput. Phys. **72**, 243 (1987).
[13] F. Jenko, Comput. Phys. Commun. **125**, 196 (2000).
[14] E. Strait, L. Lao, M. Mauel, B. Rice, T. Taylor, K. Burrell, M. Chu, E. Lazarus, T. Osborne, S. Thompson, and A. Turnbull, Phys. Rev. Lett. **75**, 4421 (1995).